

# Energy Technology

Generation, Conversion, Storage, Distribution



REPRINT

# Redox Behavior of Solid Solutions in the $\text{SrFe}_{1-x}\text{Cu}_x\text{O}_{3-\delta}$ System for Application in Thermochemical Oxygen Storage and Air Separation

Josua Vieten,<sup>\*,[a]</sup> Brendan Bulfin,<sup>[b]</sup> David E. Starr,<sup>[c]</sup> Atsushi Hariki,<sup>[d]</sup> Frank M. F. de Groot,<sup>[e]</sup> Anahita Azarpira,<sup>[c]</sup> Carolin Zachäus,<sup>[c]</sup> Michael Hävecker,<sup>[f]</sup> Katarzyna Skorupska,<sup>[f]</sup> Nicole Knoblauch,<sup>[g]</sup> Martin Schmücker,<sup>[g]</sup> Martin Roeb,<sup>[a]</sup> and Christian Sattler<sup>[a]</sup>

Perovskite oxides with temperature and oxygen partial pressure dependent non-stoichiometry  $\delta$ , such as  $\text{SrFeO}_{3-\delta}$  or its Cu-doped variants, can be applied as redox materials for two-step thermochemical processes, i.e. to reversibly store oxygen and thereby thermal energy, or separate air using concentrated solar power. We studied the redox state of Cu in  $\text{SrFe}_{1-x}\text{Cu}_x\text{O}_{3-\delta}$  samples using *in-situ* X-ray photoelectron spectroscopy (XPS) and X-ray absorption (XAS) measurements in oxygen atmospheres using synchrotron radiation, and characterized these materials through thermogravimetric analysis. By this means, we show how spectroscopic and

thermogravimetric data are correlated, suggesting that Cu and Fe are reduced simultaneously for  $x=0.05$ , whereas the reduction of samples with  $x=0.15$  is mainly driven by a change in the Fe oxidation state. Furthermore, we studied the re-oxidation kinetics of reduced  $\text{SrFe}_{1-x}\text{Cu}_x\text{O}_{3-\delta}$ , revealing very high reaction speeds with  $t_{1/2}=13$  min at  $150^\circ\text{C}$  for  $\text{SrFeO}_{3-\delta}$ . Our results indicate that  $\text{SrFe}_{1-x}\text{Cu}_x\text{O}_{3-\delta}$  solid solutions can be applied for oxygen storage and air separation with high capacity at relatively low temperatures, which allows an efficient thermochemical process.

## Introduction

Two step solar-thermochemical redox cycles using solid metal oxides as redox materials are a suitable means for solar fuel production, air separation, or energy storage. Either of these cycles share a common principle: binary or multinary oxides are heated to a certain reduction temperature  $T_{\text{red}}$  at a certain oxygen partial pressure  $p_{\text{O}_2}$  using concentrated solar radiation, at which they are partially or completely reduced under the release of pure oxygen. In a second step, these redox materials are re-oxidized using a gaseous oxidant. Possible oxidants include water or  $\text{CO}_2$ , for the production of hydrogen or carbon monoxide, respectively (see Figure 1).<sup>[2]</sup> Via this means, hydrogen for energy storage and conversion can be produced using solar energy, and syngas, a mixture of CO and  $\text{H}_2$ , can be further processed to hydrocarbons and synthetic fuels using the Fischer-Tropsch process (“solar fuels”).<sup>[3]</sup> Another application for two step solar-thermochemical cycles is the separation of air into pure oxygen and a mostly inert fraction of nitrogen, argon, and trace gases.<sup>[1,4]</sup> This application is referred to as solar-thermochemical air separation, and its potential lies in the direct usage of concentrated solar radiation as a heat source to drive this chemical separation process. Air separation is relevant for many industrial applications such as ammonia production via the Haber-Bosch process. By using solar-thermochemical redox cycles, the high electricity demand of cryogenic distillation can be avoided. Moreover, these redox materials may act as an oxygen pump, allowing the provision of low partial pressures of oxygen with an energy input significantly

lower than by using mechanical pumps.<sup>[5]</sup> Furthermore, this process can be applied for the production of high purity oxygen or for oxygen storage.

- [a] J. Vieten, Dr. M. Roeb, Prof. Dr. C. Sattler  
Institute of Solar Research  
Deutsches Zentrum für Luft- und Raumfahrt (DLR) e.V.  
Linder Höhe, D-51147 Köln, Germany  
E-mail: Josua.Vieten@dlr.de
- [b] Dr. B. Bulfin  
Professorship of Renewable Energy Carriers  
ETH Zurich  
Sonneggstr. 3, CH-8092 Zurich, Switzerland
- [c] Dr. D. E. Starr, Dr. A. Azarpira, Dr. C. Zachäus  
Institute of Solar Fuels  
Helmholtz-Zentrum Berlin für Materialien und Energie GmbH  
Hahn-Meitner-Platz 1, D-14109 Berlin, Germany
- [d] Dr. A. Hariki  
Institute for Solid State Physics  
TU Wien  
A-1040 Wien, Austria
- [e] Prof. Dr. F. M. F. de Groot  
Inorganic Chemistry & Catalysis  
Debye Institute for Nanomaterials Science, Utrecht University  
Universiteitsweg 99, Utrecht 3584 CG, The Netherlands
- [f] Dr. M. Hävecker, Dr. K. Skorupska  
Department of Inorganic Chemistry  
Fritz Haber Institute of the Max Planck Society  
Faradayweg 4–6, D-14195 Berlin, Germany
- [g] Dr. N. Knoblauch, Prof. Dr. M. Schmücker  
Institute of Materials Research  
Deutsches Zentrum für Luft- und Raumfahrt (DLR) e.V.  
Linder Höhe, D-51147 Köln, Germany

Supporting information for this article is available on the WWW under <https://doi.org/10.1002/ente.201800554>

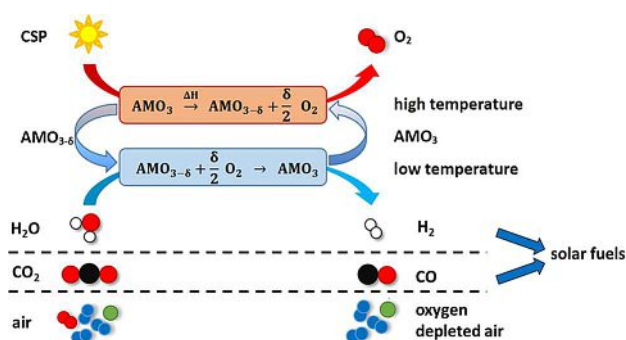


**Figure 1.** Thermochemical cycles for the production of solar fuels or for air separation. A perovskite with composition  $\text{AMO}_{3-\delta}$  is partially reduced at high temperatures and/or low oxygen partial pressures, and subsequently re-oxidized either in water,  $\text{CO}_2$ , or air. Concentrated solar power (CSP) is used as heat source, and  $\text{CO}_2$  can be combined with  $\text{H}_2$  to produce hydrocarbons ("solar fuels"). Adapted from Vieten et al.<sup>[1]</sup>

A suitable material for solar thermochemical air separation should be reducible with as little energy input as possible, which means that the redox enthalpy should be small and the entropy change upon reduction should be large, according to the Gibbs-Helmholtz equation. Potential solid oxide redox materials for these processes include binary oxides, such as  $\text{Co}_3\text{O}_4/\text{CoO}$  or  $\text{CuO}/\text{Cu}_2\text{O}$ , as well as mixed oxides containing more than one metal. Among these, perovskites constitute one of the largest groups of multinary oxides, as many different element combinations lead to stable perovskites.<sup>[6]</sup> Perovskite oxides show interesting redox properties, as many of these oxides allow a high oxygen non-stoichiometry without major changes in the crystal structure. This oxygen non-stoichiometry  $\delta$  is dependent on the temperature  $T$  and oxygen partial pressure  $p_{\text{O}_2}$ , and thus allows gradual reduction and oxidation of the perovskite in dependence of  $T$  and  $p_{\text{O}_2}$ . Perovskites of the general composition  $\text{A}^{2+}\text{M}^{3/4+}\text{O}_{3-\delta}$  with  $\delta = 0-0.5$  constitute stable phases for many different alkali earth metals A and transition metals M. The large variety of possible phases can be even extended by solid solution formation, as many of these perovskites form stable mixed phases in a large range of mixture ratios.<sup>[7]</sup>

$\text{SrFeO}_{3-\delta}$  is a simple, grossly non-stoichiometric perovskite oxide, which is well known for its oxygen non-stoichiometry and mixed +III/+IV Fe valence, which makes it a suitable

oxygen carrier for thermochemical air separation.<sup>[8]</sup> To a small extent, iron cations in this phase can be exchanged by copper cations, forming solid solutions, i.e.  $\text{SrFe}_{0.95}\text{Cu}_{0.05}\text{O}_{3-\delta}$ , as demonstrated previously by the authors.<sup>[1]</sup> This leads to an increase in the oxygen storage capacity under ambient air like conditions. However, the Cu oxidation state in these systems was yet unknown. We therefore present the results of *in-situ* X-Ray spectroscopic studies, showing that the presence of  $\text{Cu}^{3+}$  cations undergoing reduction to  $\text{Cu}^{2+}$  is most likely the case. Furthermore, the Cu content is gradually increased in order to explore the solubility limit of Cu in  $\text{SrFeO}_{3-\delta}$ , and thermogravimetric experiments have been carried out in order to study thermodynamics and kinetics of these samples, revealing very fast oxygen uptake in relaxation experiments.

## Results and Discussion

### Phase composition and solubility limits

Samples with nominal starting composition  $\text{SrFe}_{1-x}\text{Cu}_x\text{O}_{3-\delta}$  and  $x = 0-0.33$  were prepared, and their composition was studied via Energy dispersive X-Ray (EDX) analysis (see Figure 2) and X-Ray diffraction (XRD, see Figure 3). An even distribution of Cu in EDX maps as well as the presence of a single phase in the XRD analysis is a strong indicator for the formation of a solid solution. Samples with  $x = 0.05$  and  $0.15$  showed an even distribution of Cu over the measured area and a Cu content close to the expected values according to the intended phase composition. This evaluation, however, was not performed on single crystals but the cooled melt, and thus the composition measured with this method is not necessarily equal to the phase composition. Moreover, an EDX analysis of the powdered samples revealed no significant difference in the A/B site ratios between different Cu-containing samples (see supplementary information). To further evaluate the phase composition, X-Ray diffractograms were analyzed, showing no copper oxides for  $x < 0.25$  (see Figure 3). For  $\text{SrFe}_{0.95}\text{Cu}_{0.05}\text{O}_{3-\delta}$  samples, the authors previously reported the formation of a side phase with a different Sr/Fe ratio.<sup>[1]</sup> To increase the sample purity for more detailed studies, a slight Sr excess leading to a nominal starting composition of  $\text{Sr}_{1.05}\text{Fe}_{0.95}\text{Cu}_{0.05}\text{O}_{3-\delta}$  was applied. Although no

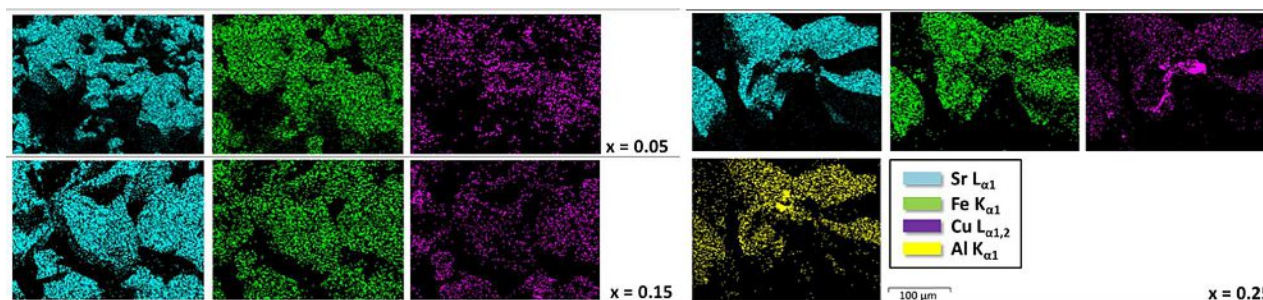


**Figure 2.** EDX maps of Cu-doped  $\text{SrFe}_{1-x}\text{Cu}_x\text{O}_{3-\delta}$  powders with the emission signals of Sr, Fe, Cu, and Al. Both Sr and Fe are evenly distributed in all cases, whereas a Cu-rich side phase is formed at  $x = 0.25$ . An Al signal was detected only at  $x \geq 0.25$ , and below the background noise level at  $x = 0.05$  and  $x = 0.15$ .

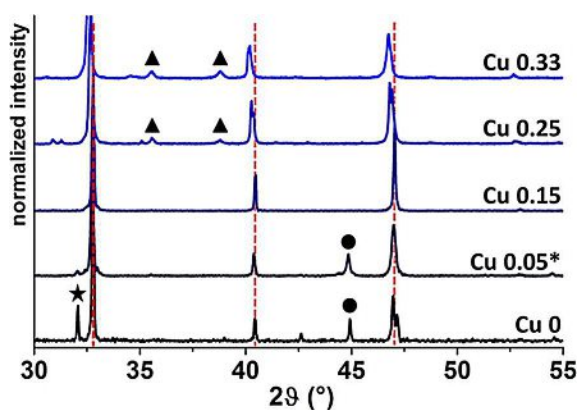


**Figure 3.** XRD analysis of  $\text{SrFe}_{1-x}\text{Cu}_x\text{O}_{3-\delta}$  powders with different Cu contents. Vertical lines are added as a guide to the eye. The reflection marked with ★ is assigned to the brownmillerite  $\text{Sr}_2\text{Fe}_2\text{O}_5$ , reflections assigned to CuO are denoted by ▲, while the origin of the reflections marked as ● is further discussed in the text. The phase marked with an asterisk was prepared using a 5% Sr excess.

significant differences in the X-Ray diffractograms were found in this case, more detailed EDX analysis on cleaved and polished pellets revealed an even distribution of Fe, Sr, and Cu throughout the sample (see supplementary information), as opposed to previous studies with no Sr excess.<sup>[1]</sup> We assume that the slight Sr excess increased the phase purity by balancing the Sr loss due to reaction with the crucible or its volatility at high temperatures, but further studies are necessary to further evaluate this point. The formation of side phases may be very susceptible to small variations in Sr content. Additionally, reflections at  $2\theta = 45^\circ$  were found in the X-Ray diffractograms of the samples with  $x = 0$  and  $x = 0.05$ , which could not be assigned to any known phase. Previous *in-situ* XRD studies showed no temperature dependent (reduction-induced) shift of this reflection, as opposed to all other reflections.<sup>[1]</sup> The authors of this previous study suspected that this reflection may be associated with the observed side phase, but as this reflection was also found in the sample prepared with slight Sr excess, the nature of this side-phase remains unclear.

Remarkably, the side phase was not formed for  $x = 0.15$ . If the Cu content was increased beyond  $x = 0.15$ , we found an uneven Cu concentration via EDX mapping of the powdered substances. Therefore, a solubility limit of Cu in  $\text{SrFe}_{1-x}\text{Cu}_x\text{O}_{3-\delta}$  of  $x \sim 0.15$  can be concluded. At  $x = 0.20$ , additional reflections were present in the X-Ray diffractograms, which potentially correspond to  $\text{Sr}_2\text{CuO}_{4-\delta}$ .<sup>[1,9]</sup> At higher Cu contents, reflections of CuO were found in the diffractograms. This is in good agreement with the phase segregation observed in the EDX maps, as well as earlier experiments by Zhang et al. on  $\text{SrFe}_{0.7}\text{Cu}_{0.3}\text{O}_{3-\delta}$  membranes, where phase segregation was observed as well.<sup>[10]</sup> Moreover, at high Cu content, aluminum was found in the samples through EDX ( $\sim 3\%$ ), which may result from partial dissolution of the alumina crucibles used for synthesis, as also described below. Excess Cu may have reacted with alumina, and ternary phases may have been formed,

which are stable according to phase diagrams of the copper oxide – alumina system.<sup>[11]</sup>

For sample preparation in a larger scale, ceramic methods involving synthesis directly from metal oxides are easier to implement. An attempt was therefore made to synthesize  $\text{SrFe}_{0.95}\text{Cu}_{0.05}\text{O}_{3-\delta}$  from  $\text{Fe}_3\text{O}_4$ ,  $\text{SrCO}_3$ , and CuO in the appropriate stoichiometric amounts by mixing the oxides and heating them in alumina crucibles using the same temperature program as for the precursors prepared via citric acid auto-combustion. The alumina crucible showed severe corrosion as a result (see supplementary information), and thermogravimetric experiments revealed lower redox mass changes than expected according to previous measurements of samples prepared via citric acid auto-combustion and subsequent high temperature treatment. However, ceramic synthesis of Cu-free  $\text{SrFeO}_{3-\delta}$  in good phase purity is possible, as demonstrated in the literature.<sup>[8b,12]</sup> It appears that the citric acid-autocombustion method is crucial to the successful preparation of  $\text{SrFe}_{0.95}\text{Cu}_{0.05}\text{O}_{3-\delta}$  solid solutions in our case, probably due to the fine dispersion of the oxide precursors resulting from auto-combustion and/or the potential formation of ternary intermediate oxides.

If oxides are used as precursors in alumina crucibles, it appears that a side reaction of CuO with  $\text{Al}_2\text{O}_3$  is more favorable than the formation of a perovskite solid solution. For instance, according to DFT calculations (the Materials Project<sup>[9b,13]</sup>), the formation of  $\text{Al}_2\text{CuO}_4$  from  $\text{Al}_2\text{O}_3$  and CuO is a possible reaction pathway, with  $\Delta H = 39 \text{ kJmol}^{-1}$ . The ceramic method, however, might be successfully applied when other crucibles are used which do not react with CuO at high temperatures, i.e. platinum crucibles.

#### Oxygen storage capacity and thermodynamics

Although the response to changes in temperature and oxygen partial pressure in the thermobalance is very similar for all samples, the changes in non-stoichiometry, and, associated with that, the changes in oxygen storage capacity show some differences. If the temperature is swept between 400 and 900 °C while the oxygen partial pressure is kept at 2 mbar at the high temperature step and 900 mbar at the low temperature step, all materials show a gravimetric oxygen storage capacity between 18 and 19 litres  $\text{O}_2$  (ideal gas, SATP) per kg of redox material, and some lower capacities if the temperature or pressure differences are lower (see supplementary information). When the oxygen storage capacities are compared to  $\text{SrFeO}_{3-\delta}$  as a reference, an increase in capacity through Cu doping is visible in most cases (see Figure 4). Whereas the sample with 5% Cu on the Fe sites shows advantages at lower temperatures and high oxygen partial pressures, the sample with higher Cu content has a significantly increased oxygen storage capacity at high temperatures and low partial pressures. This sample showed a change in non-stoichiometry of  $\Delta\delta = 0.35$  between 350 °C at  $p_{\text{O}_2} = 0.9 \text{ bar}$  and 1000 °C at  $p_{\text{O}_2} = 1 \cdot 10^{-4} \text{ bar}$ , which is not possible with pure  $\text{SrFeO}_{3-\delta}$ .<sup>[8a,14]</sup> However, when comparing the redox

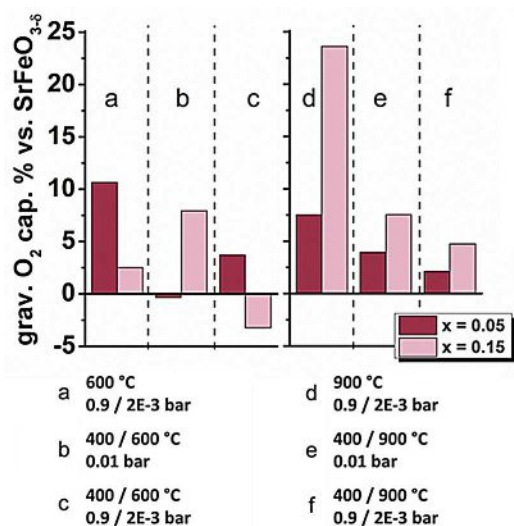


**Figure 4.** Percentage difference in gravimetric oxygen storage (mol O<sub>2</sub>/g of redox material) of Cu-doped SrFeO<sub>3-δ</sub> vs. pure SrFeO<sub>3-δ</sub> extracted from thermogravimetric data. Temperature, oxygen partial pressure, or both were changed according to the annotations (a) to (f). Cu doping leads to an increase in oxygen storage capacity in most cases. The material with lower Cu content performs better at low temperature, whereas the oxygen storage capacity of the material with  $x=0.15$  is higher at high temperatures and lower oxygen partial pressures.

thermodynamics using a van't Hoff approach, the observed differences are very small (see supplementary information). Considering the measurement uncertainties, it is difficult to determine significant differences between the samples, especially when considering that the redox enthalpy and entropy may be coupled when determined through this approach (enthalpy-entropy compensation<sup>[15]</sup>). The observed redox enthalpies, however, are in good agreement with literature data for the reduction of SrFeO<sub>3</sub> to Sr<sub>2</sub>Fe<sub>2</sub>O<sub>5</sub> and Sr<sub>2</sub>Cu<sub>2</sub>O<sub>5</sub> to SrCuO<sub>2</sub>, which have been determined using DFT to be 84 and 82.5 kJ per mol of O, respectively.<sup>[9b,13]</sup> The differences in redox extent between the three samples gained via isothermal and isobaric variation of the equilibrium conditions vary significantly, indicating potential changes in redox entropy upon Cu doping, as the entropic term in the Gibbs-Helmholtz equation depends only on the temperature, whereas the overall Gibbs free energy depends on both temperature and oxygen partial pressure. From the point of view of statistical thermodynamics, it is likely that changes occur upon partial substitution of one species in the lattice by another, as the amount of distinct sites for the oxide ions is changed. However, further measurements of thermodynamic properties need to be carried out in order to give a definitive answer. In conclusion, the observed differences in oxygen storage capacity arise from small changes in the redox thermodynamics upon substitution of Fe by Cu in the perovskite lattice.

### Redox kinetics

Cu doping of SrFeO<sub>3-δ</sub> has a significant influence on the redox reaction kinetics. In particular, we could observe major differences in the reaction rates at low temperatures in our relaxation experiments (see supplementary information). SrFeO<sub>3-δ</sub> can be re-oxidized at low temperatures. In fact, even at 150 °C substantial re-oxidation can be observed within minutes, and the state of half oxidation is reached after  $t_{1/2} = 13$  min. These particularly fast reaction rates are strongly related to the high oxide ion conductivity in the perovskite lattice, and the very similar crystal structures of the oxidized and reduced phases. These fast redox reactions and their phase stability constitute one of the main advantages when using perovskites for thermochemical air separation instead of stoichiometric redox pairs such as the CuO/Cu<sub>2</sub>O or the Co<sub>3</sub>O<sub>4</sub>/CoO system.<sup>[1,16]</sup> For thermodynamic reasons, re-oxidation at low temperatures is associated with a very low equilibrium oxygen partial pressure. In contrast to the undoped sample, the oxidation of SrFe<sub>0.85</sub>Cu<sub>0.15</sub>O<sub>3-δ</sub> does not reach the state of half oxidation even after one hour of oxidation at 150 °C. At higher temperatures above approx. 300 °C, no significant differences in oxidation kinetics could be observed between the three samples. Using the half-lives  $t_{1/2}$  of the reactions, it is possible to create an Arrhenius-like plot of  $\ln t_{1/2}$  vs.  $1/T$  (see Figure 5). Two different regimes can

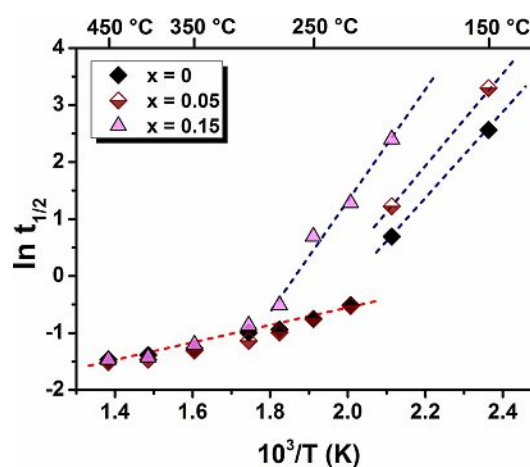


**Figure 5.** The natural logarithm of the reaction half-lives  $t_{1/2}$  of oxidation reactions performed on different SrFe<sub>1-x</sub>Cu<sub>x</sub>O<sub>3-δ</sub> samples with  $x=0$ , 0.05, and 0.15 vs.  $1/T$ . Half-lives were determined through relaxation experiments in a thermobalance. The red dashed line indicates a gas transport limited regime and the blue dashed lines indicate an activation limited regime. Cu doping decreases the oxidation speed at low temperatures.

be distinguished. At high temperatures and all three samples show very similar reaction rates, and the influence of a temperature change on the reaction speed is smaller than at low temperatures.

This behavior can be explained if the reaction is controlled by the diffusion of oxygen to the samples in the reaction medium. As the flow of oxygen inside the thermogravimetric analyzer is limited, a certain reaction speed cannot

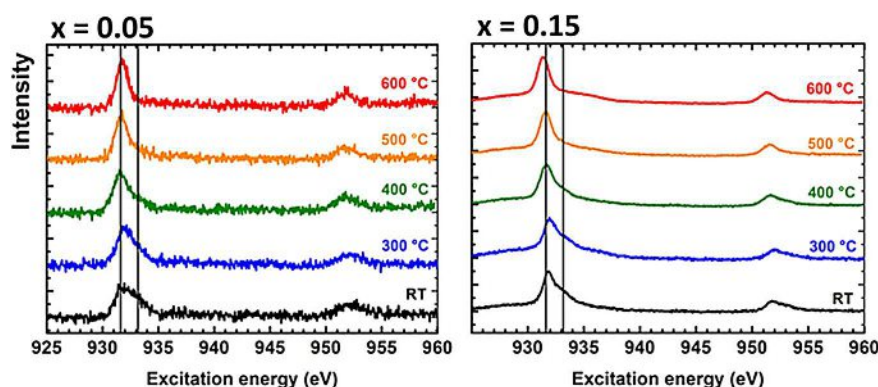


**Figure 6.** Cu 2p XAS spectra of the  $\text{SrFe}_{1-x}\text{Cu}_x\text{O}_{3-\delta}$  samples with  $x=0.05$  (left) and  $x=0.15$  (right) at different temperatures in pure oxygen atmospheres with  $p=1.0$  mbar. The peak broadening at low temperature with features at higher excitation energies indicates the formation of a second Cu species through oxidation. Vertical lines are added as a guide to the eye.

be exceeded. This also indicates that the observed half-lives of about 20 seconds could even be lower if the gas flow rates were increased. Conversely, the reaction rate is more temperature dependent at lower temperatures. We explain the observed behavior with a transition from diffusion/mass transport control to activation control at low temperatures. Samples with higher Cu content show slower reaction rates than those with lower or no Cu. The transition point between the two regimes also shifts to higher temperatures with increasing Cu content. The partial replacement of Fe ions by Cu might impede the diffusion of oxide ions through the lattice to some extent, or the surface reaction may become the rate determining step. Further clarification of the rate-limiting step requires more detailed studies of the reaction kinetics in the future. Moreover, the oxygen diffusivity in samples with different Cu concentration can be measured in further experiments. For the application as redox materials for solar-thermochemical air separation or oxygen pumping, our results indicate that a) the reaction rates are very high compared to stoichiometric oxides, allowing many redox cycles per time unit and high air separation rates, and b) that samples with lower Cu content are more suitable redox materials at temperatures lower than  $\sim 300^\circ\text{C}$ .

#### Redox state of Cu and XPS/XAS spectra

As explained in the previous two sections, the partial substitution of Fe by Cu in  $\text{SrFeO}_{3-\delta}$  samples influences their redox performance. To elucidate possible reasons for this effect, the replacement of Fe ions by copper ions in the lattice is investigated via near ambient pressure XPS, which is a method to study these redox reactions *in-situ*.

Of particular interest is the redox state of Cu in these samples. Whereas in  $\text{SrFeO}_{3-\delta}$  the Fe ions are present in a mixed valence state of  $\text{Fe}^{4+}$  and  $\text{Fe}^{3+}$  (depending on the reduction extent), the formation of  $\text{Cu}^{4+}$  is significantly less common.<sup>[17]</sup> Higher valence states of Cu than  $\text{Cu}^{3+}$  have so far only been observed in metal complex compounds prepared in the presence of strong oxidants, and there are indications of  $\text{Cu}^{4+}$  at high

oxygen pressures in some perovskites.<sup>[18]</sup>  $\text{SrCuO}_3$  and its reduction to the brownmillerite phase  $\text{Sr}_2\text{Cu}_2\text{O}_5$  can be studied theoretically via DFT calculations (the Materials Project<sup>[9b,13]</sup>). It is predicted that  $\text{SrCuO}_3$  forms a (slightly distorted) perovskite structure similar to the one of  $\text{SrFeO}_3$ , but due to the negative reaction enthalpy for reduction to the brownmillerite phase,<sup>[9a,13]</sup> extremely high oxygen partial pressures would be required to stabilize such a phase. This would also apply to a solid solution of  $\text{SrCuO}_{3-\delta}$  and  $\text{SrFeO}_{3-\delta}$ , as long as the two phases can be treated as individual sub-lattices. It can therefore be assumed that Cu would be present in the  $\text{Cu}^{3+}$  state under the conditions we applied. As the  $\text{Cu}^{3+}$  in perovskite-like structures can easily be thermally reduced to  $\text{Cu}^{2+}$  ( $\Delta H_{\text{red}}$  (per mol of O) for the reduction of  $\text{Sr}_2\text{Cu}_2\text{O}_5$  to  $\text{SrCuO}_2$ : 82.5 kJ/mol), it is likely to observe a reduction of  $\text{Cu}^{3+}$  to  $\text{Cu}^{2+}$ .

By studying the X-Ray absorption (XAS) *in-situ* in dependence of the temperature at near-ambient oxygen pressures, we are able to draw some first conclusions on the Cu redox state in our compounds (see Figure 6). The Cu  $L_{3-}$  edge typically ranges around 931–934 eV in perovskites.<sup>[19]</sup> Indeed, we observed a single peak at 931.8 eV excitation energy for both  $x=0.05$  and  $x=0.15$  in  $\text{SrFe}_{1-x}\text{Cu}_x\text{O}_{3-\delta}$  at a temperature of  $600^\circ\text{C}$  in 1.0 mbar oxygen atmosphere. At lower temperatures, the absorption feature broadens towards higher excitation energies, indicating the formation of a second species with higher valence state which generates a signal at about 933 eV. Moreover, the lower Cu content of the sample with  $x=0.05$  with respect to  $x=0.15$  becomes obvious, as the signal intensity is much lower and the signal to noise ratio is decreased. We attribute the generation of the second peak to the oxidation of the sample in the oxygen atmosphere at lower temperatures due to a shift of the chemical equilibrium between the perovskite and the brownmillerite state, and we will use the XPS spectra in the following to elucidate the formal valence state of Cu in these compounds. The Cu  $2p_{3/2}$  XPS spectra (see Figure 7) show temperature dependent changes which are very similar as those in the XAS spectra.

A second peak at higher binding energy becomes clearly visible as the temperature is reduced, especially at  $300^\circ\text{C}$  and

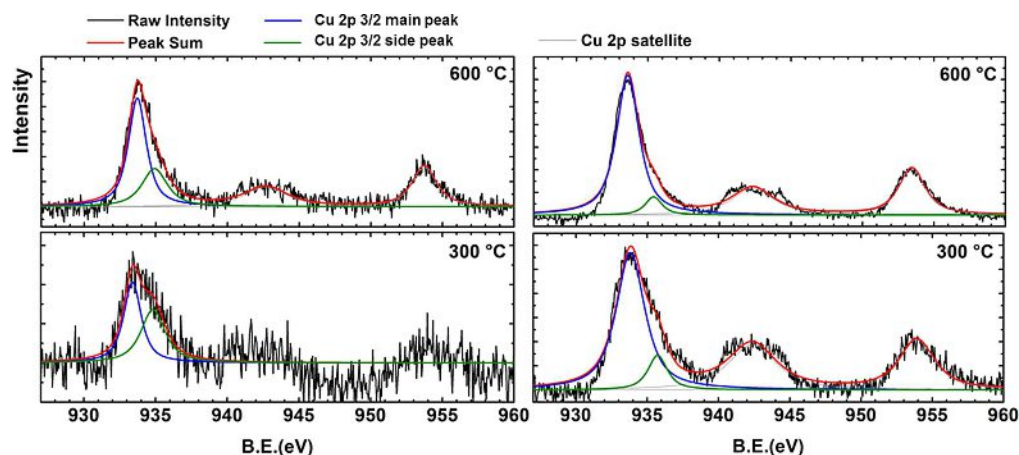


**Figure 7.** Cu  $2p$  XPS spectra recorded in 1.0 mbar O<sub>2</sub> atmospheres using SrFe<sub>1-x</sub>Cu<sub>x</sub>O<sub>3-δ</sub> samples with  $x=0.05$  (left) and  $x=0.15$  (right). The main peak with lowest B.E. shows a shoulder at higher B.E. which is attributed to the generation of Cu<sup>3+</sup> states. Its intensity decreases with increasing temperature due to the thermal reduction of the samples. Moreover, the lower intensity and the higher separation of this shoulder for  $x=0.15$  from the main peak indicate that this system in general shows a more Cu<sup>2+</sup>-like character than the  $x=0.05$  system.

RT (see supplementary information). We note that a measurement at RT was only possible for SrFe<sub>1-x</sub>Cu<sub>x</sub>O<sub>3-δ</sub> samples with  $x=0.15$  due to high absorption from dense oxygen gas at low temperatures. The Cu  $2p_{3/2}$  XPS main peak is located at  $933.42 \pm 0.20$  eV (B.E.) and  $933.71 \pm 0.11$  eV for  $x=0.05$  and  $x=0.15$ , respectively. In contrast to the main line, the peak at higher binding energy shows notable Cu-content dependence. This peak has higher intensity and is located at a lower B.E. in  $x=0.05$  than in  $x=0.15$  (for  $x=0.15$ , B.E. =  $935.61 \pm 0.18$  eV, for  $x=0.05$ , B.E. =  $934.75 \pm 0.17$  eV). This leads to a larger splitting between the main and high binding energy peaks for higher Cu content. The high binding energy peak increases in intensity at low temperature for both cases (see supplementary information). In the case of  $x=0.15$ , two distinct (but overlapping) peaks are observed, whereas for  $x=0.05$  the high binding energy peak is observed as a shoulder on the main peak. The binding energy positions of the peaks we observed, however, may be sensitive to the specific curve fitting procedure. The 933 eV B.E. of the main line is characteristic of a Cu<sup>2+</sup> system, while the peak around 935 eV is a signature of the Cu<sup>3+</sup> system in the ground state.<sup>[20]</sup> Thus, the Cu-content dependence of the high binding energy peak intensity in a wide temperature range suggests that in SrFe<sub>0.85</sub>Cu<sub>0.15</sub>O<sub>3-δ</sub> the Cu is in a more Cu<sup>2+</sup>-like state, whereas in the  $x=0.05$  system there is a higher fraction of Cu in the Cu<sup>3+</sup> state. The high binding energy peak position is sensitive to the charge transfer energy (of the Cu<sup>3+</sup> state<sup>[20a]</sup>). The peak structure we observed is similar to the one seen in a study by Meyers et al., where perovskites with mixed Cu<sup>3+</sup> and Cu<sup>2+</sup> valence states have been studied.<sup>[20b]</sup> The decrease in intensity of the high binding energy peak with increasing temperature (see Figure 8) can be associated with the thermal reduction of the system, leading to the generation of oxygen vacancies and the reduction from Cu<sup>3+</sup> to Cu<sup>2+</sup>, as already suggested in the XAS data analysis.

Similar Cu  $2p_{3/2}$  XPS spectra can be observed for YBa<sub>2</sub>Cu<sub>3</sub>O<sub>7-δ</sub> annealed at different temperatures, showing a

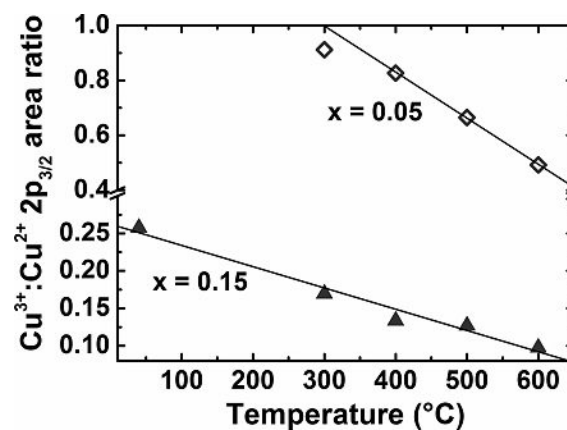


**Figure 8.** Temperature dependence of the  $2p_{3/2}$  XPS peak area ratios between high energy shoulder and the main peak measured under constant oxygen pressure  $p=1.0$  mbar for SrFe<sub>1-x</sub>Cu<sub>x</sub>O<sub>3-δ</sub> samples. The sample with  $x=0.05$  shows a stronger temperature dependence of the peak area ratios, indicating a stronger effect of thermal reduction of the samples on the Cu redox state. Lines are added as a guide to the eye, indicating a near-linear dependence of the peak area ratios on the temperature.

different extent of oxygen non-stoichiometry and a change in the Cu<sup>3+</sup> peak intensity at high B.E.<sup>[21]</sup> These conclusions are further supported by the behavior of the so-called shake-up or satellite peaks, which can clearly be observed in all of our Cu  $2p$  XPS spectra at about 942–943 eV B.E. These can only occur if empty states in the Cu  $d$ -band are available, which is not the case for Cu<sup>0</sup> and Cu<sup>+</sup>.<sup>[22]</sup> As we always observed satellite peaks, we can exclude the presence of pure Cu<sup>+</sup> in our structures.<sup>[19b]</sup> The intensity of these shake-up peaks is a measure of the amount of empty  $d$  states in Cu, and is therefore related to the oxidation state. By analyzing the ratio of the shake-up peak integral area vs. the main peak area (see supplementary information), we can conclude that a relatively high formal Cu oxidation state must be present in our samples, similar as in LaCuO<sub>3-δ</sub> or NaCuO<sub>2</sub>, as shown in the literature.<sup>[23]</sup> The satellite vs.  $2p_{3/2}$  main peak intensity

decreases from over 50 % to 36 % upon reduction at higher temperatures for  $x=0.15$ . In contrast, no clear temperature-dependent trend of the peak area ratios could be observed for  $x=0.05$ , most likely due to the low signal to noise ratio associated with the low Cu content of these samples.

We could not find evidence for the presence of a formal Cu oxidation state higher than +3. Although the relatively high binding energies we found are in good agreement with the studies presented by Darracq et al.,<sup>[18a]</sup> the observed peak structure can be best explained with a mixture of  $\text{Cu}^{3+}$  and  $\text{Cu}^{2+}$  states, as described before. By combining data from thermogravimetric analysis (TGA) and XPS studies, it is possible to draw some conclusions on the reduction process depending on the Cu content of the studied  $\text{SrFe}_{1-x}\text{Cu}_x\text{O}_{3-\delta}$  samples. Figure 9 shows a plot of the change in oxygen non-

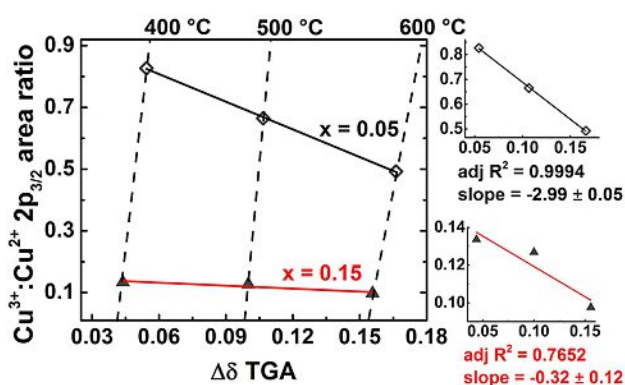


**Figure 9.** Correlation between the change in non-stoichiometry  $\Delta\delta$  (reference  $\Delta\delta=0$ :  $p_{\text{O}_2}=0.18$  bar,  $400^\circ\text{C}$ ) extracted via thermo-gravimetric analysis (TGA) and the Cu  $2p_{3/2}$  XPS area ratio between the high B.E. shoulder and the main peak and in  $\text{SrFe}_{1-x}\text{Cu}_x\text{O}_{3-\delta}$  samples with  $x=0.05$  and  $x=0.15$  at different temperatures and  $p=1.0$  mbar (XPS) and  $p_{\text{O}_2}=2$  mbar (TGA). Dashed isothermal lines are added as a guide for the eye. A linear fit of the data shows a strong correlation between the Cu redox extent expressed through the XPS peak area ratio and the oxygen release of the whole sample for  $x=0.05$ , whereas for  $x=0.15$  the correlation is much less expressed, indicating the presence of mostly passive  $\text{Cu}^{2+}$  ions in this case.

stoichiometry  $\Delta\delta$  extracted from TGA measurements vs. the  $2p_{3/2}$  Cu XPS main vs. shoulder peak area ratio. TGA data was taken for an oxygen partial pressure  $p_{\text{O}_2}=2$  mbar, which is closest to the conditions during the *in-situ* XPS measurements in oxygen atmospheres with  $p=1.0$  mbar. For  $x=0.05$ , we could find a clear linear dependence of the peak area ratios on the change in oxygen non-stoichiometry. This was not the case for  $x=0.15$ , where the adjusted  $R^2$  of a linear fit was significantly smaller than in the case of the samples with 5 % Cu substitution. Moreover, the slope of the linear fit is about one order of magnitude smaller in this case. As discussed earlier, the  $2p_{3/2}$  peak area ratio between main and high binding energy peak in Cu XPS can be seen as a measure of the  $\text{Cu}^{3+}/\text{Cu}^{2+}$  ratio. Therefore, in the case of  $x=0.05$ , the change in oxygen non-stoichiometry is associated with a major change in  $\text{Cu}^{3+}$  content. As this change in redox extent cannot be explained by just the reduction of  $\text{Cu}^{3+}$  to  $\text{Cu}^{2+}$  (a full reduction of all Cu in the sample would only correspond to

$\Delta\delta=0.025$ ), this result means that  $\text{Fe}^{4+}$  and  $\text{Cu}^{3+}$  are reduced at the same time to a large extent. In contrast, the oxygen release of the sample with  $x=0.15$  does not lead to major changes in the Cu redox state, meaning that the reduction of  $\text{SrFe}_{0.85}\text{Cu}_{0.15}\text{O}_{3-\delta}$  is mainly driven by the reduction of  $\text{Fe}^{4+}$ , whereas most of the copper is passive in the  $\text{Cu}^{2+}$  state. This means in conclusion that the  $x=0.05$  sample can be best described as  $\text{SrFe}_{0.95}\text{Cu}_{0.05}\text{O}_{3-\delta}$ , whereas the  $x=0.15$  sample would be more accurately represented by  $(\text{SrFe}_{1-x}\text{Cu}_x\text{O}_{3-\delta})_x \cdot (\text{SrCuO}_2)_{x-x'}$  with  $x'$  denoting a small amount of Cu being involved in the redox process.

The XPS studies on the reduction process of  $\text{SrFe}_{1-x}\text{Cu}_x\text{O}_{3-\delta}$  samples are completed by analysis of the spectra of other elements (see supplementary information). As explained in the experimental section, carbonaceous species on the surface have been reduced successfully by initially heating the samples to  $T < 300^\circ\text{C}$  in oxygen atmosphere, yielding no detectable C 1s signal after this treatment. Moreover, a characteristic O 1s signal can be observed. Very similar to studies on  $\text{Ca}_{0.8}\text{Sr}_{0.2}\text{MnO}_{3-\delta}$  presented by the authors previously, a distinct surface oxygen species with higher binding energy can be observed next to an oxygen species characteristic for the bulk in samples with Cu content  $x=0.05$ .<sup>[24]</sup> By scanning the samples at constant temperature and oxygen pressure with different excitation energies, different sample depths could be scanned, and the surface species was clearly identified (see supplementary information). Afterwards, a measurement at different temperatures with constant excitation energy and oxygen pressure has been conducted, which shows that the relative intensity of the surface species decreased with respect to the bulk species with increasing temperature, i.e., increasing reduction extent. This result is again very similar to the one observed in  $\text{Ca}_{0.8}\text{Sr}_{0.2}\text{MnO}_{3-\delta}$  and most probably indicates that the surface of the sample is reduced preferentially. In addition, Fe  $2p$  XPS spectra were studied, but as described in the literature, no significant changes in the peak shapes and intensities are expected between  $\text{Fe}^{3+}$  and  $\text{Fe}^{4+}$  species.<sup>[25]</sup> Exemplary XPS spectra for  $\text{SrFe}_{0.85}\text{Cu}_{0.15}\text{O}_{3-\delta}$  are presented in the supplementary information, revealing in fact no major difference between spectra recorded at different temperatures, i.e., different reduction extents. Further studies with other techniques may be used to evaluate the Fe redox states in these materials, such as Mössbauer spectroscopy.<sup>[26]</sup>

## Conclusions

We present an extensive study of the  $\text{SrFe}_{1-x}\text{Cu}_x\text{O}_{3-\delta}$  system and redox reactions induced in these samples upon thermal reduction and subsequent re-oxidation. Our results indicate that solid solution phases are formed for  $x \leq 0.15$ . Cu-containing phases could not be prepared via a ceramic method from strontium carbonate and the metal oxides, in contrast to pure  $\text{SrFeO}_{3-\delta}$ . The oxygen storage capacity can be improved by Cu doping of  $\text{SrFeO}_{3-\delta}$ , and we present experimental data on the effect of different temperature and oxygen partial pressure levels on the reduction extent. However, the replacement of Fe by Cu in the lattice decreases

the oxidation speed at low temperatures, as shown through our kinetic studies. The re-oxidation of our samples can be completed in less than 20 s at temperatures above 300–350 °C, and SrFeO<sub>3-δ</sub> still shows decent re-oxidation speeds at temperatures as low as 150 °C, which are comparable with the re-oxidation speeds of stoichiometric oxides at much higher temperatures. This is particularly helpful if very low oxygen partial pressures shall be reached in thermal air separation and oxygen pumping processes. From the thermogravimetric studies, it can be concluded that samples with high Cu content can be applied best at high temperatures and low oxygen partial pressures, whereas those with lower Cu content show better redox performance at lower temperatures. The redox properties were studied more in detail via *in-situ* XPS and XAS measurements using synchrotron radiation. It has been shown that the reduction process of Cu ions in the lattice is associated with a change of the Cu oxidation state from +3 to +2. Whereas in the case of  $x=0.05$  the reduction process is characterized by a mostly simultaneous reduction of Fe<sup>4+</sup> and Cu<sup>3+</sup>, the reduction of the samples with  $x=0.15$  is mainly driven by the reduction of Fe species. From this, it may be concluded that these samples are more accurately represented by (SrFe<sub>1-x</sub>Cu<sub>x</sub>O<sub>3-δ</sub>)<sub>x</sub>·(SrCuO<sub>2</sub>)<sub>x-x'</sub>. The formation of a layered structure like this would also yield one possible explanation for the limited oxygen diffusion in these samples at low temperatures through impeding diffusion, but further studies are necessary to confirm this hypothesis. All in all, SrFeO<sub>3-δ</sub> is an excellent candidate as a material for application in solar thermochemical air separation, oxygen storage, and oxygen pumping processes and the replacement of some of the Fe by Cu can be beneficial for its redox performance, depending on the desired application.

## Experimental Section

All samples are prepared via a citric acid auto-combustion route, as described in the literature.<sup>[1,27]</sup> 5.00 mmol of SrFe<sub>1-x</sub>Cu<sub>x</sub>O<sub>3-δ</sub> solid solutions are prepared by mixing 50 ml of an aqueous 0.1 M Fe(NO<sub>3</sub>)<sub>3</sub> solution (from Fe(NO<sub>3</sub>)<sub>3</sub>·9 H<sub>2</sub>O, VWR Chemicals, 99.0–101.0 %) with Cu(NO<sub>3</sub>)<sub>2</sub> (from Cu(NO<sub>3</sub>)<sub>2</sub>·2.5 H<sub>2</sub>O, Sigma Aldrich, 98 %) and 4 mL of a 2.5 M citric acid solution (from anhydrous citric acid, Merck, 99 %). 0.738 g (5.00 mmol) of SrCO<sub>3</sub> (99.99 %, Alfa Aesar) are then added as a Sr source. The starting mixture for the SrFeO<sub>3-δ</sub> reference sample is prepared in a similar manner, but instead of SrCO<sub>3</sub>, 50 ml of a 0.1 M Sr(NO<sub>3</sub>)<sub>2</sub> solution (from Sr(NO<sub>3</sub>)<sub>2</sub>, Alfa Aesar, >99.0 %) are used, leading to the same final Sr concentration. The mixtures are heated to the boiling point and most of the water is evaporated until a gel forms, which is then further heated to 200 °C remove the remaining water. Subsequently, the reaction vessel is heated first to 300 °C, then after a few minutes to 500 °C on a hot plate until the auto-combustion reaction occurs. The remaining finely dispersed oxide powder is ground and mixed and then filled into open alumina crucibles for the subsequent high temperature synthesis. The samples are treated for 10 h at 800 °C twice with an intermediate cool-down step followed by a high temperature step at 1300 °C for 20 h, as described previously by the authors.<sup>[1,28]</sup> Intermediate mixing steps are not necessary. After the high temperature treatment, the samples are ground to form a powder. Alternatively, a solid state synthesis method is tested for the

preparation of SrFe<sub>0.95</sub>Cu<sub>0.05</sub>O<sub>3-δ</sub> on the scale of 1–5 g perovskite material. SrCO<sub>3</sub> (Alfa Aesar, 99 %; Ba 1 %, –325 mesh), Fe<sub>3</sub>O<sub>4</sub> (Alfa Aesar, 97 %, –325 mesh), and CuO (Cerametec Materials, 99.99 %, –200 mesh) are mixed in a pestle according to the intended stoichiometry ratio and accounting for the mass loss due to the de-carbonization of SrCO<sub>3</sub> at elevated temperatures. The samples are heated twice to 800 °C for 10 h and once to 1300 °C for 20 h, as described above for the precursors prepared via the Pechini method.

The formation of solid solutions is studied using X-Ray diffraction (XRD) and energy dispersive X-Ray spectroscopy (EDX). For XRD, the powdered samples are analyzed on Si single crystals using Cu K<sub>α</sub> radiation in a Siemens D-5000 diffractometer. An angular range of  $2\theta=10-90^\circ$  is scanned in steps of 0.02° with 6 seconds measurement time per step. The undoped reference sample, SrFeO<sub>3-δ</sub>, is studied using a Bruker D8 Advance diffractometer equipped with an area detector (steps of 0.03° with 2.5 seconds per step). Moreover, a Zeiss Ultra-55 SEM system is used for EDX analysis using an Oxford INCA® X-Ray detector. Before EDX analysis is carried out, the powdered samples are sputter-coated with Pt for 15 sec in order to increase their electric conductivity. Furthermore, for a more accurate phase analysis of the sample with  $x=0.05$  we use pellets annealed for 10 h at 1300 °C in a muffle furnace which are then cleaved, polished, and sputter-coated with Pt.<sup>[1]</sup>

Thermogravimetric analysis is performed using powdered samples (100–450 mg) on flat ceramic sample holders covered by Pt foil on the surface. A STA 449 F3 Jupiter thermobalance by Netzsch is used in combination with a combined oxygen sensor and oxygen pump manufactured by SETNAG. Argon 5.0 (Linde), synthetic air (80:20 mol % N<sub>2</sub>:O<sub>2</sub>, Linde) and oxygen 5.0 (Linde) are used as the gas feedstock and the mass flow of the gases is controlled via the mass flow controllers of the thermobalance, allowing to reach different oxygen partial pressures depending on the mixture ratios. The oxygen partial pressure is monitored at the outlet of the thermobalance using a combined oxygen pump and sensor manufactured by SETNAG. A silicon carbide furnace is used within the thermobalance to heat the samples to different temperature levels at a maximum heating rate of 50 K min<sup>-1</sup>. Data on redox thermodynamics is obtained via the van't Hoff method by measuring the mass change at equilibrium at different temperature and oxygen partial pressure levels, as described in the literature.<sup>[24,29]</sup> Relaxation experiments in order to determine the re-oxidation speed are carried out by heating the samples to 860 °C under Ar and allowing them to cool to different temperature levels while Ar flow is maintained. Once the lower temperature level is reached, the atmosphere is switched by adding oxygen and an oxygen partial pressure of 0.9 bar is reached, allowing for quick re-oxidation. For the kinetics studies, exactly 260.0 mg of powdered samples are used in each measurement to exclude potential differences in gas flow rates and diffusion lengths.

The oxidation state of the samples under redox conditions is studied using near ambient pressure X-Ray spectroscopy (NAP-XPS) using the ISSISS beamline at the X-Ray source BESSY II, Helmholtz-Zentrum Berlin (HZB), Germany, as described in the literature.<sup>[24]</sup> Pure oxygen atmospheres of up to 1.0 mbar are used (oxygen partial pressure equals total pressure), and pellets of the samples are prepared via compression of the powders. The samples are heated via an infrared laser, reaching temperatures of up to 700 °C (pyrometer and type K thermocouple readings). Carbonaceous species on the surface are removed by initially heating the samples to >300 °C in 1.0 bar O<sub>2</sub> (see supplementary information). To exclude systematic errors of the peak shifts, the signal is compared to the Sr 1s XPS signal and its second

order peaks. To monitor potential surface alterations to beam damage, the O 1s XPS signal was observed at each temperature step. The data is evaluated using the software *SpecsLab Prodigy* and *XPSPeak 4.1*. After subtracting a Shirley type background, peaks are fit using symmetric mixed Lorentzian-Gaussian functions (80% Lorentzian). XAS (measured as total electron yield, TEY) measurements are carried out under the same conditions. In this case, the peak positions are calibrated using the mirror currents.

## Acknowledgements

This work has received funding from the Helmholtz Association within the Virtual Institute SolarSyngas (VH-VI-509) and the project DÜSOL (EFRE-0800603) which is co-funded in the Klimaschutzwettbewerb "ErneuerbareEnergien.NRW" by the state of Northrhine-Westphalia, Germany, and the European EFRE fund. We thank HZB for the allocation of synchrotron radiation beamtime.

## Conflict of Interest

The authors declare no conflict of interest.

**Keywords:** solar thermochemistry · strontium ferrite · air separation · oxygen storage · perovskites

- [1] J. Vieten, B. Bulfin, F. Call, M. Lange, M. Schmucker, A. Francke, M. Roeb, C. Sattler, *J. Mater. Chem. A* **2016**, *4*, 13652–13659.
- [2] a) W. C. Chueh, C. Falter, M. Abbott, D. Scipio, P. Furler, S. M. Haile, A. Steinfield, *Science* **2010**, *330*, 1797–1801; b) A. Steinfield, *Sol. Energy* **2005**, *78*, 603–615.
- [3] M. Roeb, C. Sattler, R. Klüser, N. Monnerie, L. de Oliveira, A. G. Konstandopoulos, C. Agrafiotis, V. T. Zaspalis, L. Nalbandian, A. Steele, P. Stobbe, *J. Sol. Energy Eng.* **2005**, *128*, 125–133.
- [4] M. Ezbiri, K. M. Allen, M. E. Gálvez, R. Michalsky, A. Steinfield, *ChemSusChem* **2015**, *8*, 1966–1971.
- [5] S. Brendelberger, H. von Storch, B. Bulfin, C. Sattler, *Sol. Energy* **2017**, *141*, 91–102.
- [6] A. A. Emery, J. E. Saal, S. Kirklin, V. I. Hegde, C. Wolverton, *Chem. Mater.* **2016**, *28*, 5621–5634.
- [7] J. Vieten, B. Bulfin, M. Senholdt, M. Roeb, C. Sattler, M. Schmücker, *Solid State Ionics* **2017**, *308*, 149–155.
- [8] a) Y. Takeda, K. Kanno, T. Takada, O. Yamamoto, M. Takano, N. Nakayama, Y. Bando, *J. Solid State Chem.* **1986**, *63*, 237–249; b) M. Schmidt, S. J. Campbell, *J. Phys. Chem. Solids* **2002**, *63*, 2085–2092; c) E. Marek, W. Hu, M. Gaultois, C. P. Grey, S. A. Scott, *Appl. Energy* **2018**, *223*, 369–382.
- [9] a) A. Jain, G. Hautier, C. J. Moore, S. Ping Ong, C. C. Fischer, T. Mueller, K. A. Persson, G. Ceder, *Comput. Mater. Sci.* **2011**, *50*, 2295–2310; b) A. Jain, S. P. Ong, G. Hautier, W. Chen, W. D. Richards, S. Dacek, S. Cholia, D. Gunter, D. Skinner, G. Ceder, K. A. Persson, *APL Materials* **2013**, *1*, 011002; c) R. C. Lobo, F. J. Berry, C. Greaves, *J. Solid State Chem.* **1990**, *88*, 513–519.
- [10] H. Zhang, T. Wang, X. Dong, W. Lin, *J. Nat. Gas Chem.* **2009**, *18*, 45–49.
- [11] K. T. Jacob, C. B. Alcock, *J. Am. Ceram. Soc.* **1975**, *58*, 192–195.
- [12] E. A. Filonova, A. N. Demina, E. A. Kleibbaum, L. Y. Gavrilova, A. N. Petrov, *Inorg. Mater.* **2006**, *42*, 443–447.
- [13] A. Jain, G. Hautier, S. P. Ong, C. J. Moore, C. C. Fischer, K. A. Persson, G. Ceder, *Phys. Rev. B* **2011**, *84*, 045115.
- [14] M. Schmidt, *J. Phys. Chem. Solids* **2000**, *61*, 1363–1365.
- [15] R. R. Krug, W. G. Hunter, R. A. Grieger, *Nature* **1976**, *261*, 566.
- [16] T. Block, M. Schmücker, *Sol. Energy* **2016**, *126*, 195–207.
- [17] W. Levason, M. D. Spicer, *Coord. Chem. Rev.* **1987**, *76*, 45–120.
- [18] a) S. Darracq, S. G. Kang, J. H. Choy, G. Demazeau, *J. Solid State Chem.* **1995**, *114*, 88–94; b) X. J. Wu, P. Laffez, H. Yamauchi, N. Mōri, *Physica C* **1994**, *228*, 292–298.
- [19] a) E. Sacher, J. E. Klemberg-Sapieha, A. Cambron, A. Okoniewski, A. Yelon, *J. Electron Spectrosc. Relat. Phenom.* **1989**, *48*, C7–C12; b) Z. Qing, Y. Yun-Yu, D. Jian-Hong, S. Xi, H. Zhi-Wei, Y. Jun-Ye, W. Qing-Tao, Y. Ri-Cheng, L. Xiao-Dong, L. You-Wen, *Chin. Phys. Phys. Lett.* **1999**, *25*, 020701; c) K. Karlsson, O. Gunnarsson, O. Jepsen, *Phys. Rev. Lett.* **1999**, *82*, 3528–3531.
- [20] a) K. Okada, A. Kotani, *J. Phys. Soc. Jpn.* **1999**, *68*, 666–673; b) D. Meyers, S. Mukherjee, J. G. Cheng, S. Middey, J. S. Zhou, J. B. Goodenough, B. A. Gray, J. W. Freeland, T. Saha-Dasgupta, J. Chakhalian, *Sci. Rep.* **2013**, *3*, 1834; c) D. D. Sarma, O. Strebel, C. T. Simmons, U. Neukirch, G. Kaindl, R. Hoppe, H. P. Müller, *Phys. Rev. B* **1988**, *37*, 9784–9787.
- [21] P. Steiner, S. Hübner, V. Kinsinger, I. Sander, B. Siegwart, H. Schmitt, R. Schulz, S. Junk, G. Schwitzgebel, A. Gold, C. Politis, H. P. Müller, R. Hoppe, S. Kemmler-Sack, C. Kunz, *Z. Phys. B Con. Mat.* **1988**, *69*, 449–458.
- [22] S. Poulston, P. M. Parlett, P. Stone, M. Bowker, *Surf. Interface Anal.* **1996**, *24*, 811–820.
- [23] a) M. Karppinen, H. Yamauchi, H. Suematsu, K. Isawa, M. Nagano, R. Itti, O. Fukunaga, *J. Solid State Chem.* **1997**, *130*, 213–222; b) K. Karlsson, O. Gunnarsson, O. Jepsen, *J. Phys. Condens. Matter* **1992**, *4*, 2801.
- [24] B. Bulfin, J. Vieten, D. E. Starr, A. Azarpira, C. Zachäus, M. Haevecker, K. Skorupska, M. Schmücker, M. Roeb, C. Sattler, *J. Mater. Chem. A* **2017**.
- [25] A. Nening, A. K. Opitz, C. Rameshan, R. Rameshan, R. Blume, M. Hävecker, A. Knop-Gericke, G. Rupprechter, B. Klötzer, J. Fleig, *J. Phys. Chem. C* **2016**, *120*, 1461–1471.
- [26] P. Ravindran, R. Vidya, H. Fjellvåg, A. Kjekshus, *Phys. Rev. B* **2008**, *77*, 134448.
- [27] a) A. E. Danks, S. R. Hall, Z. Schnepf, *Mater. Horiz.* **2016**, *3*, 91–112; b) F. Deganello, G. Marci, G. Deganello, *J. Eur. Ceram. Soc.* **2009**, *29*, 439–450; c) M. P. Pechini, **1966**.
- [28] J. Vieten, B. Bulfin, M. Roeb, C. Sattler, *Solid State Ionics* **2018**, *315*, 92–97.
- [29] B. Bulfin, L. Hoffmann, L. de Oliveira, N. Knoblauch, F. Call, M. Roeb, C. Sattler, M. Schmucker, *Phys. Chem. Chem. Phys.* **2016**, *18*, 23147–23154.

Version of record online: December 5, 2018